minerals

MDPI

Article

Enhanced Flotation of Dolomite Particles by Grinding with Short Cylindrical Media

Shuai Ren, Cong Wang, Zhiyong Gao and Shihong Xu *

School of Minerals Processing and Bioengineering, Central South University, Changsha 410083, China; 195606039@csu.edu.cn (S.R.); cong_wang@csu.edu.cn (C.W.); zhiyong.gao@csu.edu.cn (Z.G.)
* Correspondence: shihong.xu@csu.edu.cn

Abstract: In the field of mineral processing, the successful flotation of target minerals requires sufficient liberation through grinding. The aim of this paper is to compare and evaluate the performance of ball versus short cylindrical media for comminution of dolomite by point and line contact, respectively. The results of the grinding experiments indicate that short cylinders generate more angular particles with intermediate sizes and exhibit a higher grinding efficiency compared to balls. The Population Balance Model demonstrates the distribution of broken fragment sizes during the breaking stage for each size range. The results of the DEM (discrete element method) grinding simulation are consistent with the experimental findings in terms of the distribution of particle sizes, the shape of the particles, and the distribution of broken fragment sizes. Furthermore, short cylinders selectively produce more active {104} crystal surface of dolomite, which possess a higher adsorption capacity with collectors and are preferentially floated as the concentrate. In reverse flotation for removal of dolomite, tests confirm that the products obtained from grinding with short cylinders exhibit a higher flotation recovery of dolomite compared to those obtained from ball grinding. This study provides a reference scheme for optimizing the grinding and flotation processes of valuable minerals.

Keywords: grinding media; dolomite; Population Balance Model; DEM grinding simulation; particle reactivities; flotation behaviors

Citation: Ren, S.; Wang, C.; Gao, Z.; Xu, S. Enhanced Flotation of Dolomite Particles by Grinding with Short Cylindrical Media. *Minerals* **2023**, *13*, 1550. https://doi.org/10.3390/min13121550

Academic Editor: Dave Deglon

Received: 13 November 2023
Revised: 8 December 2023
Accepted: 13 December 2023
Published: 15 December 2023

1. Introduction

Phosphate rock plays a crucial role as a primary source of phosphorus in the agricultural and chemical industries. Over 90% of the current application of phosphorus resources is in the form of agricultural fertilizer, of which more than 80% originates from fossil sources [1,2]. Apatite, comprising fluorapatite, hydroxylapatite, and chlorapatite, is a commonly occurring mineral in nature that is rich in phosphorus [1]. In addition, dolomite is the main gangue mineral associated with apatite [3]. Reverse flotation is the primary technique employed for the separation of apatite and dolomite [4–8]. Hence, enhancing the flotation recovery of dolomite can facilitate the separation and purification of apatite, thereby playing a crucial role in the effective exploitation of phosphorus resources.

The recovery rate of dolomite is primarily influenced by the flotation reagent used. Sodium oleate is employed as a collector, while phosphoric acid acts as an inhibitor for apatite. These chemicals were frequently used in the process of separating phosphate rock in industrial manufacturing [8–11]. However, despite the use of efficient chemicals, the brittleness and ease of grinding of dolomite make it challenging to recycle the resulting fine particles. Hence, the phosphate industry has long been separating and discarding fine particles as a common practice, leading to substantial losses in the form of slimes.

Optimizing grinding technology is the primary approach to decrease the percentage of small particle sizes. The grinding media system holds the primary variable factor during the grinding process. The particle size distribution is affected by the shape of the grinding media, thus greatly influencing the interaction between the grinding media and the ores. Short cylindrical media have a larger surface area than spherical media with similar mass and size [12–14]. It is widely recognized that increasing the surface area of the grinding media improves the chances of breaking the ore. Point and line contacts in short cylinders help to preferentially grind larger particles. When the line area captures larger particles, it effectively prevents further fragmentation of smaller particles, as in rod mills [13]. The shape of the grinding media also affects the morphology of particles. The shape of particles varies depending on the type of grinding media—particles produced through short cylinder grinding media are more elongated due to abrasion and chipping, while those produced through ball grinding media have a more circular shape due to impact processes [15,16]. Angular particles show greater tendencies to float than rounded particles, as the absence of edges in the latter makes it challenging for them to adhere to bubbles [17,18]. Consequently, the use of short cylinder grinding media has the potential to minimize excessive grinding and boost the proportion of elongated particles that demonstrate enhanced floatability properties.

The choice of grinding media significantly influences the proportions of crystal surface exposure, as shown in Table 1. In research carried out by Gao [16,19], it was proven that rod milling induces an enhanced exposure of {101} crystal surface on scheelite particles, whereas ball milling leads to a heightened exposure of {001} crystal surface on scheelite particles. When using a rod as grinding media, fluorite showcases a higher exposure of crystal surfaces such as {110} and {310}, while using spherical media leads to a greater exposure of {111} crystal surface. For chalcopyrite, the use of a short cylindrical media exposes a more highly active {112} crystal surface, whereas spherical media exposes a more low-activity crystal surface such as {220} [20]. Meng et al. [21] demonstrated that corundum balls displayed a higher level of exposure of the {110} crystal surface of spodumene due to an increased concentration of active Al sites, in contrast to agate balls. As a result, the use of short cylinder grinding media can enhance the exposure of highly active crystal surfaces, thereby improving their floatability.

Table 1. Influence of the grinding media on the exposure ratio of the crystal surface.

Mineral	Grinding Media	More Exposed Crystal Surfaces
scheelite	rod	{101}
scheelite	ball	{001}
fluorite	rod	{110} and {310}
fluorite	ball	{111}
chalcopyrite	short cylinder	{112}
chalcopyrite	ball	{220}
spodumene	corundum ball	{110}
spodumene	agate ball	{010}

This study explores the properties of dolomite grinding products by employing short cylinders and balls as the media for grinding. The research involves conducting grinding experiments, analyzing the distribution of particle sizes, calculating using the Population Balance Model, measuring through SEM (scanning electron microscope), simulating grinding using DEM (discrete element method), conducting X-ray diffraction (XRD) measurements, and performing crystal chemistry calculations. Flotation experiments were performed on individual minerals and mixed ore samples to confirm the dolomite's ability to float when short cylinders were used, and its performance was compared to that of balls.

2. Materials and Methods

2.1. Materials and Reagents

The dolomite specimen was acquired from Dianchi, Yunnan Province, China. The purity of the dolomite sample was determined to be 99.2% by chemical analysis. The dolomite was crushed using a JC6 jaw crusher to a size smaller than 1 mm before being utilized for grinding. The grinding feed consists of particles that are sieved out and range in size from 0.6 mm to 1 mm.

Aladdin Reagent Company supplied sodium oleate and phosphoric acid, both with a purity exceeding 98%, for their respective roles as a collector and inhibitor. The pH of the pulp was adjusted using hydrochloric acid and sodium hydroxide. Deionized water, with a resistivity surpassing 18 MΩ × cm, was employed.

2.2. Grinding Studies

A homemade drum mill was used for pure mineral grinding experiments. The grinding chamber has a diameter of 50 mm and a length of 100 mm. We employed two different types of stainless steel grinding media, short cylinders, and balls, during the grinding process. The media filling ratios in the tests were 43%, 45%, and 48%, respectively. The ratios of grinding media with diameters of 10 mm, 5 mm, and 2 mm were determined to be 4:3:3 and 5:3:2, respectively, in grinding experiments. The equipment and grinding media employed in the experimental procedure are consistent with the findings of earlier investigations [19,20].

In each grinding test, the grinding chamber is filled with 35 g of mineral sample. Subsequently, 19 milliliters of purified water are introduced to achieve a pulp concentration of 65%. The rotational speed of the mill has been adjusted to 120 revolutions per minute. After the specified grinding time elapses, the final product is rinsed using deionized water and then subjected to filtration. The samples resulting from the process of grinding are then utilized for subsequent evaluation and experimentation.

For grinding products above 400 mesh, the standard Taylor Sieve grading method is used for particle size analysis. In addition, for products with particle sizes below 400 mesh, the MalvernMASTERSIZER2000 particle size analyzer (Malvern Instruments Ltd, Malvern City, UK) is used for testing and analysis. This particle size analyzer is equipped with a Hydro2000MU(A) feeder (Malvern Instruments Ltd, Malvern City, UK) and can measure particles in the size range of 0.02 to 2000 μm.

2.3. Population Balance Model

Population Balance Model for batch milling describes the change in mass fraction of each size range with time. This model includes two functions: the selection function (S) and the breakage distribution function (B). The selection function (S) represents the rate at which each size range of the mineral is broken, while the breakage distribution function (B) represents the size distribution of the breakage products for a specific particle size. The classical expression for the Population Balance Model is given as follows:

$$\frac{dw_i}{dt} = -s_i w_i + \sum_{j=1}^{i} b_{ij} s_j w_j \tag{1}$$

In this equation, the variable "t" signifies time, while the subscripts "i" and "j" symbolize different particle size ranges, which are classified from coarsest (1) to finest (6). The letter "s_i" represents the specific rate at which particles in the "i-th" size range break. The b_{ij} denotes the mass fraction of "i-th" size range in the broken product of the "j-th" size range.

Assuming that the selection function matrix S and the breakage distribution matrix B were time-independent, one can solve Equation (1).

$$\frac{dW}{dt} = AW \tag{2}$$

$$C = (B - I)SS = \begin{bmatrix} s_1 & & & & \\ & s_2 & & & \\ & & s_3 & & \\ & & & \ddots & \\ & & & & s_n \end{bmatrix}$$

$$B = \begin{bmatrix} & & & & & \\ b_{21} & & & & & \\ b_{31} & b_{32} & & & & \\ b_{41} & b_{42} & b_{43} & & & \\ \vdots & \vdots & \vdots & \ddots & & \\ b_{n1} & b_{n2} & b_{n3} & \dots & b_{n\ n-1} & \end{bmatrix}$$

Henri Berthiaux [22] devised a technique to find the solution to Equation (2).

Assuming that S is independent of time, Equation (2) represents an n-dimensional linear homogeneous differential equation that can be solved using the diagonalization method. C is a lower triangular matrix, hence it can be diagonalized, with its eigenvalues being its diagonal elements. Therefore, there exists an invertible matrix P,

$$S = -P^{-1}CP \tag{3}$$

$$\frac{dW}{dt} = -PSP^{-1}W \tag{4}$$

Assuming $W = PZ$, where Z is a column matrix, then

$$P\frac{dZ}{dt} = -PSP^{-1}PZ \tag{5}$$

i.e.,

$$\frac{dZ}{dt} = -SZ \tag{6}$$

Since S is a diagonal matrix, Equation (6) is easy to integrate,

$$Z = \mu_D E_s(t) \tag{7}$$

where, μ_D is the diagonal matrix of the integral constant and $E_s(t)$ is the column matrix composed of $\exp(-s_i t)$.

Let the transformation matrix $T = P\mu_D$, and the diagonal elements of T are the same as μ_D, then

$$W = TE_s(t) \tag{8}$$

The Equation (8) is expanded at the size range. For example, $w_1(t)$ is the mass fraction of minerals of a size range 1 at a grinding time t, and t_{11} is an element of the first row and column of the T matrix.

$$\begin{bmatrix} w_1(t) = t_{11}\exp(-s_1 t) \\ w_2(t) = t_{21}\exp(-s_1 t) + t_{22}\exp(-s_2 t) \\ w_3(t) = t_{31}\exp(-s_1 t) + t_{32}\exp(-s_2 t) + t_{33}\exp(-s_3 t) \\ \vdots \\ w_n(t) = t_{n1}\exp(-s_1 t) + t_{n2}\exp(-s_2 t) + \ldots + t_{nn}\exp(-s_n t) \end{bmatrix} \tag{9}$$

By means of Equations (2) and (3), there is a formula available.

$$B = I - PSP^{-1}S^{-1} \tag{10}$$

The parameters T and S can be obtained by fitting the experimental data using the Levenberg–Marquardt algorithm. Then P can then be calculated by $T = P\mu_D$. Ultimately, the breakage distribution function B can be determined by employing Equation (10).

2.4. SEM Analysis

The grinding products underwent pre-treatment procedures to ensure accurate observation and analysis. The dried sample was kept in a controlled environment at room temperature. In the sample holder, the sample was placed on a conductive fabric. The formation of a layer of particles occurs subsequently. The sample was then subjected to SEM test with a spot size of 2.5 nm, a high voltage of 12.5 kV, and a magnification of 400×.

The properties of the particles, including their length (L), width (W), area (A), perimeter (Pe), roundness (Ro), and elongation (E), were assessed by utilizing ImageJ software (version 1.53f51) for analysis. Our team has developed the calculation method by building upon the extensive research conducted earlier [19,20].

2.5. DEM Grinding Simulation

The DEM was first introduced by Cundall and Strack [23] as a simulation technique that allows for the virtual replication of particle movement and interaction. Using Newton's second law of motion and contact models in both the vertical and horizontal directions, it is possible to calculate paths for every individual particle [24]. The method mentioned here is especially useful in dealing with problems concerning granular materials and is commonly used in simulations within the comminution industry [25].

Rocky DEM software (version 2022 R1.2) was utilized to conduct a simulation on DEM grinding. The breakage model opted for was Ab-T10, with a minimum absolute size of 10 μm. The distribution model utilized was Gaudin–Schumann. All parameters, including the grinding chamber, grinding media, ore, and other factors, remained consistent with the original experimental setup. The state of motion of the spherical and short cylindrical media of the software is shown in Figure 1.

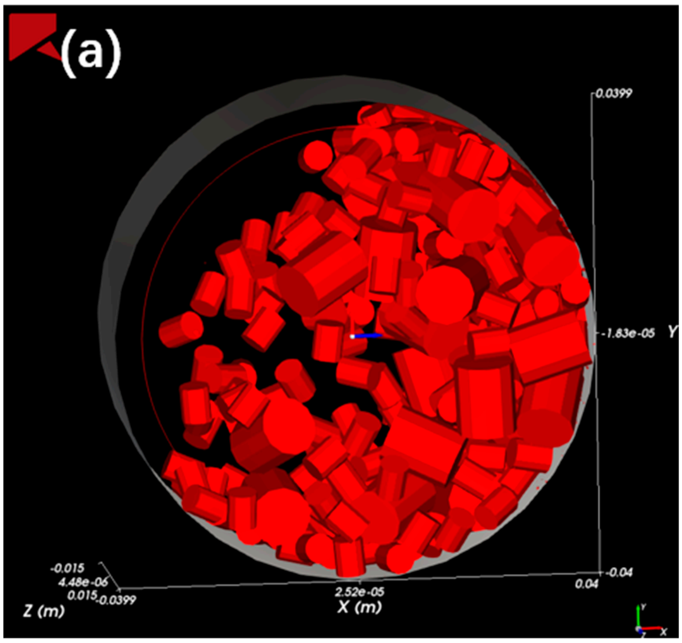

Figure 1. *Cont.*

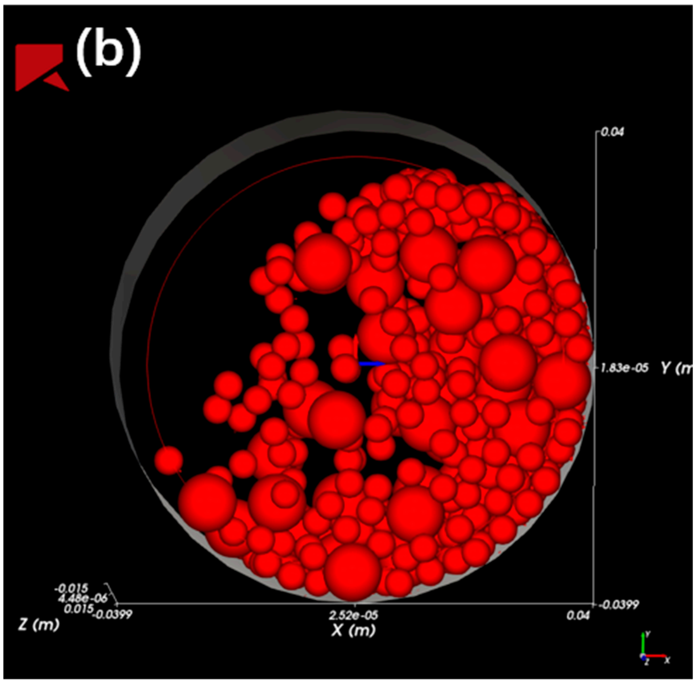

Figure 1. DEM grinding simulation using short cylinder (**a**) and ball (**b**) as grinding media.

Given the software's lack of the sphericity parameter, I proactively utilized the "Custom Property" function to create the "*sphericity*" element.

$$Sphericity = \frac{\left(36\pi V^2\right)^{1/3}}{A_s} \tag{11}$$

where V denotes the volume of the particle, A_s denotes the surface area of the particle.

To compute the PBM based on the simulated data results, the "Particles In Mass" and "Particles Out Mass" values extracted from the "Time Plot" were employed. The parameter "Particles Out Mass" indicates the cumulative mass of all particles and fragments that have been expelled from the selection within a specific time interval, whereas "Particles In Mass" denotes the contrary situation.

Using the illustration of b_{32}'s computation as a demonstration:

$$O_{-0.6+0.15} = O_2(1 - b_{32}) + O_3 \tag{12}$$

where b_{32} denotes the mass fraction of the size range 3 in the broken product of the size range 2, $O_{-0.6+0.15}$ denotes the "Particles Out Mass" of particles at a size of −0.6 + 0.15 mm, O_2 denotes the "Particles Out Mass" of particles at a size of −0.6 + 0.3 mm, and O_3 denotes the "Particles Out Mass" of particles at a size of −0.3 + 0.15 mm.

i.e.,

$$b_{32} = 1 - \frac{\left(O_{-0.6+0.15} - O_3\right)}{O_2} \tag{13}$$

2.6. XRD Analysis

The XRD analysis was conducted with a D8-ADVANCE Bruker-AKS instrument (Bruker, Karlsruhe, Germany) in the reflection mode. A Cu Kα radiation with a wavelength of 1.5406 Å was utilized, along with a tube potential of 40 mV and a tube current of 40 mA. The goniometer speed was set at 2°/min. To eliminate bias, the samples were prepared in a manner that ensured random orientation.

2.7. Crystal Chemistry Calculations

MaterialStudio software (version 19.1.0.2353) was used to build mineral protocells corresponding to XRD crystal parameters. After that, the number and density of exposed metal atoms on these crystal surfaces were calculated [26]. Utilizing CASTEP modules, we employed the PBE function to approximate the exchange-dependent potential of the GGA in calculating the surface energy of diverse dolomite crystal surfaces. The energy cutoff for the plane wave calculations was set at 820.0 eV. The k-point grids used for the structural calculations were $2 \times 1 \times 1$. The energy tolerance, force tolerance, and displacement tolerance were defined as 2.0×10^{-5} eV/atom, 0.05 eV/Å, and 0.002 Å, respectively [5,27].

$$E_{surf} = \frac{\left[E_{slab} - \left(\frac{N_{slab}}{N_{bulk}}\right)E_{bulk}\right]}{2A_z} \tag{14}$$

The E_{slab} and E_{bulk} represent the total energy, while N_{slab} and N_{bulk} represent the total number of atoms in the crystal surface model and unit cell, respectively. A_z denotes the area of the surface model along the z-axis direction.

2.8. Flotation Tests

The flotation tests for a specific mineral were conducted using an XFG flotation machine at an impeller speed of 1700 rpm. The 2 g ground particles in the size range of −74 + 38 µm were combined with 35 mL of deionized water. The resulting mixture was then transferred to a 40 mL flotation cell and stirred for 1 min. The pH of the slurry was adjusted using either sodium hydroxide (NaOH) or hydrochloric acid (HCl) solution. Then, sodium oleate solution with a concentration of 2×10^{-4} mol/L was added, and the flotation process lasted for 3 min. Subsequently, the flotation product was filtered, dried, weighed, and finally, its recovery was calculated. The flotation tests were repeated three times and the average recovery was calculated as the final result. The flow is shown in Figure 2.

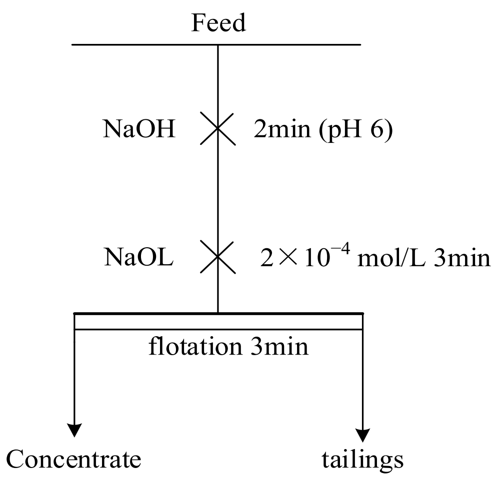

Figure 2. The flotation flowsheet of the single ore.

3. Results

3.1. Grinding Test Results

The ores were commonly ground to particles measuring around −74 µm to release valuable minerals [28,29]. According to Gontijo and Ahn [28,30], it was found that a particle size range of −74 + 10 µm is optimal for the flotation procedure. The utilization of the −74 µm and −74 + 10 µm percentages was carried out to assess the grinding efficiency and effectiveness. Initially, the two media proportions tested were 5:3:2 and 4:3:3 in terms of mass ratios using a filling ratio of 45%. Figure 3a displays the correlation between the grinding time and the percentage of particles with a size of −74 µm. The distribution of media in a ratio of 5:3:2 led to a higher percentage of particles with a size of −74 µm compared to a ratio of 4:3:3, regardless of whether short cylinders or balls were used. Similarly, the media proportion of 5:3:2 is found to have a greater impact on −74 + 10 µm values compared to the proportion of 4:3:3, as shown in Figure 3b. Conversely, Figure 3c reveals that the media proportion of 5:3:2 has a lesser effect on −10 µm values in comparison to the proportion of 4:3:3. Consequently, there is a notable difference in the influence of media proportion on particle sizes based on the different ratios examined. The media's ratio of 5:3:2 was selected as the optimal choice for conducting additional tests.

In addition, the filling ratio during the grinding process was optimized and the corresponding results are shown in Figure 4. The results show that for short cylinders and spheres, the percentage of −74 µm and −74 + 10 µm are the lowest at a filling ratio of 43%. The experimental results for 45% and 48% fill ratios are very close. Considering that higher filling ratios lead to an increase in energy consumption, a 45% filling ratio was selected as the most favorable.

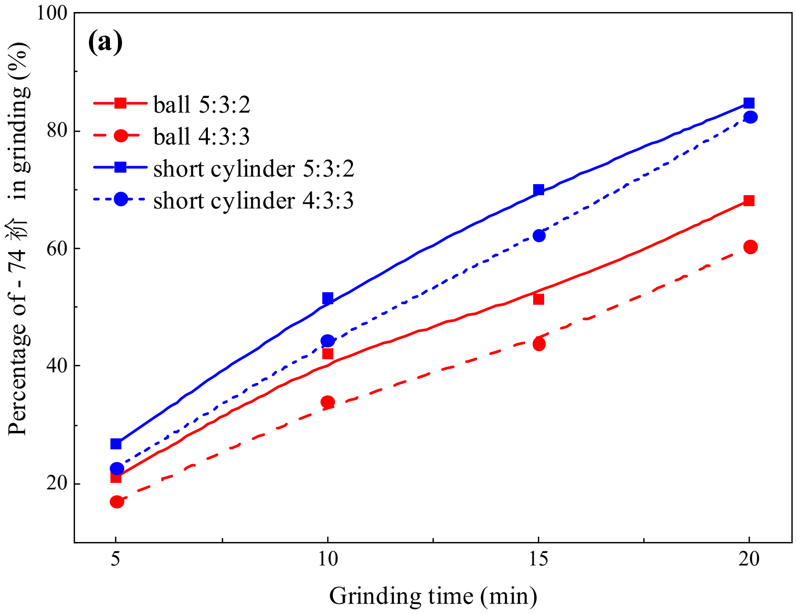

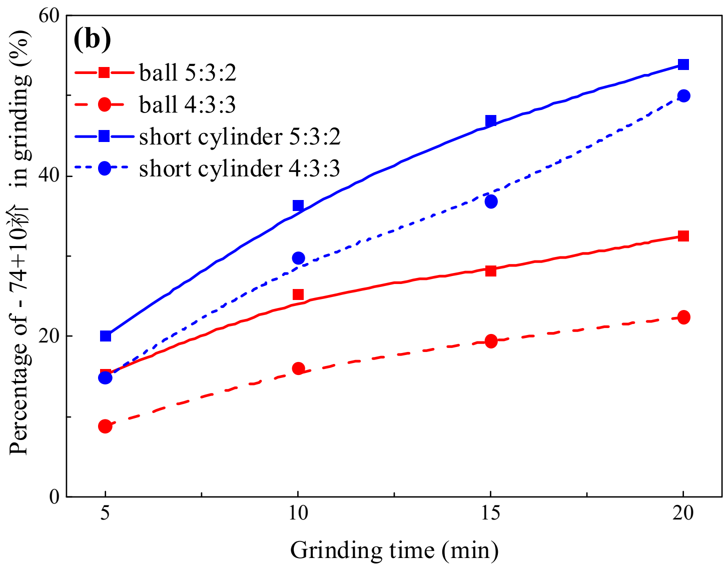

Figure 3. *Cont.*

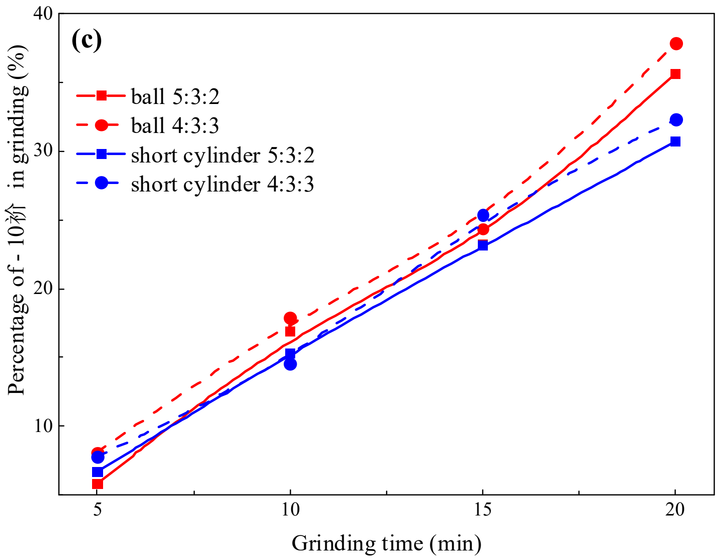

Figure 3. The percentage of −74 µm (**a**) and −74 + 10 µm (**b**) and −10 µm (**c**) of dolomite at different grinding time using the two media proportions with the mass ratios of 5:3:2 and 4:3:3.

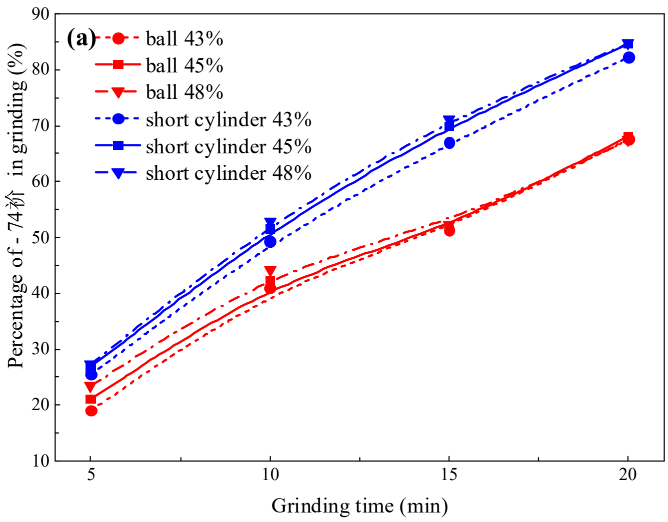

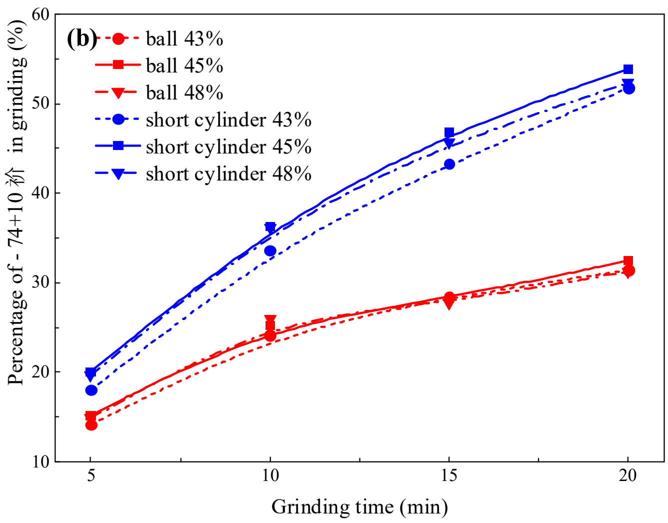

Figure 4. *Cont.*

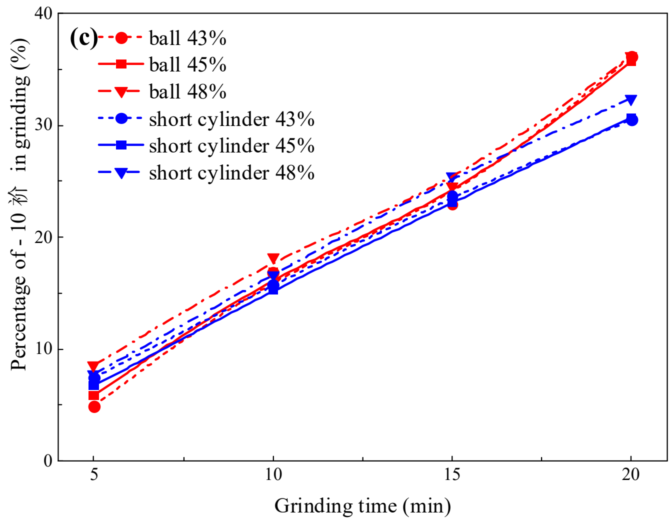

Figure 4. The percentage of −74 µm (**a**) and −74 + 10 µm (**b**) and −10 µm (**c**) of dolomite at different grinding times using three filling ratios of 43%, 45%, and 48%.

3.2. Particle Size Distribution Analysis

Different types of grinding media have been discovered to produce specific physical and chemical attributes in the ground products, such as particle sizes and shapes [31,32]. In light of this, the subsection aimed to examine the particle size distribution of fluorapatite and dolomite products when employing short cylinders and balls as grinding media at different grinding durations. The obtained results, as depicted in Figures 5 and 6, were analyzed and summarized. The grinding products obtained from using short cylinders showed lower percentages of +74 µm and −10 µm fractions compared to the ones obtained from using balls. Furthermore, the proportion of particles measuring −74 + 10 µm was higher when short cylinders were used instead of balls. This implies that using short cylinders as the media is beneficial for minimizing both larger and smaller particles, enhancing grinding efficiency, and preventing excessive grinding resulting in increased overall productivity.

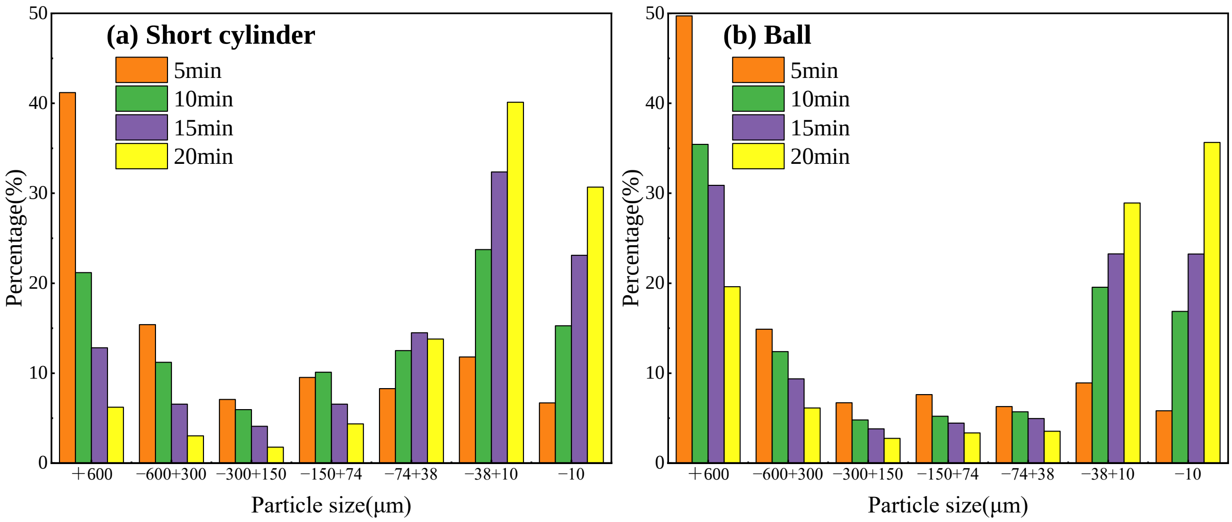

Figure 5. Particle size distribution of dolomite products at different grinding times using short cylinder (**a**) and ball (**b**) as grinding media.

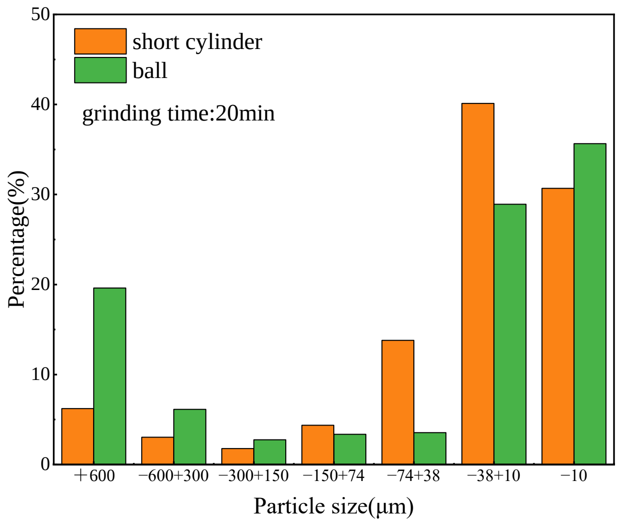

Figure 6. Particle size distribution of dolomite products at 20 min using short cylinder and ball as grinding media.

3.3. Population Balance Model

The minerals are categorized into six size ranges: 1: −1000 + 600 μm, 2: −600 + 300 μm, 3: −300 + 150 μm, 4: −150 + 74 μm, 5: −74 + 10 μm, 6: −10 μm. The grades are assigned as 1, 2, 3, 4, 5, and 6, respectively. Since b_{65} is constant at 1, only the first four size ranges were tested for single-range grinding, respectively.

Four feed samples were prepared from the first four size ranges, each containing only a single size range, and four grinding tests were performed. The obtained grinding test results are subsequently employed to compute the Population Balance Model. Hence, Tables 2 and 3 show the fragmentation distributions in the short cylinder and ball-milled samples of dolomite, respectively.

Table 2. The fragmentation distribution of the dolomite grinding product using short cylinder as grinding media.

	Feed (μm) / Product (μm)	−1000 + 600	−600 + 300	−300 + 150	−150 + 74	−74 + 10	−10
Short cylinder	−1000 + 600	0	0	0	0	0	0
	−600 + 300	0.531	0	0	0	0	0
	−300 + 150	0.196	0.202	0	0	0	0
	−150 + 74	0.225	0.122	0.335	0	0	0
	−74 + 10	0.048	0.327	0.222	0.821	0	0
	−10	0	0.35	0.443	0.179	1	1

Table 3. The fragmentation distribution of the dolomite grinding product using ball as grinding media.

	Feed (μm) / Product (μm)	−1000 + 600	−600 + 300	−300 + 150	−150 + 74	−74 + 10	−10
Ball	−1000 + 600	0	0	0	0	0	0
	−600 + 300	0.409	0	0	0	0	0
	−300 + 150	0.362	0.158	0	0	0	0
	−150 + 74	0.129	0.139	0.348	0	0	0
	−74 + 10	0.1	0.314	0.118	0.764	0	0
	−10	0	0.389	0.534	0.236	1	1

After consulting Tables 2 and 3, it has been observed that the proportion of −74 + 10 μm in the fragmentation distribution of short cylinder grinding products is larger than that of ball milling, and the proportion of −10 μm is smaller than that of ball milling. This means that coarse particles have a greater chance of generating intermediate grades after being ground by the short cylindrical media.

3.4. SEM Analysis

Previous research has stressed the importance of considering particle morphology in mineral flotation, as illustrated in studies [15,33]. The shapes of dolomite particles, which were ground using short cylinders and balls, were analyzed using SEM. The SEM images show distinct differences in particle morphology between the ones produced by ball milling, which appear more rounded, and the ones generated by short cylinder milling, which exhibit a more elongated shape with pronounced edges.

Statistical morphology parameters were calculated to offer a broader depiction of the differences in particle shapes produced by using spherical and short cylindrical media. The results are showcased in Table 4. The measurements revealed that the short cylinder grinding products displayed a greater elongation measure but a lesser roundness measure when compared to the ball grinding products.

Table 4. Average values of morphology parameters of the ground dolomite particles.

Grinding Media	Number	*L* (μm)	*W* (μm)	*A* (μm^2)	*Pe* (μm)	*E*	*Ro*
Short cylinder	220	69.617	46.312	2624.989	192.369	1.536	0.856
Ball	220	77.822	56.725	3718.272	221.670	1.394	0.883

In addition, to confirm the precision of the mentioned morphology, 300 dolomite particles were chosen for statistical analysis and curve fitting through the GaussAmp method in Origin 2021 software. The roundness and elongation of the mill product particles are shown in Figures 7a and 7b, respectively. It is evident from Figure 7 that the Ro and E values for dolomite particles after being ground by short cylinders were measured to be 0.855 and 1.350. The Ro and E values for particles ground using balls were measured to be 0.899 and 1.321. These findings closely align with the data provided in Table 4.

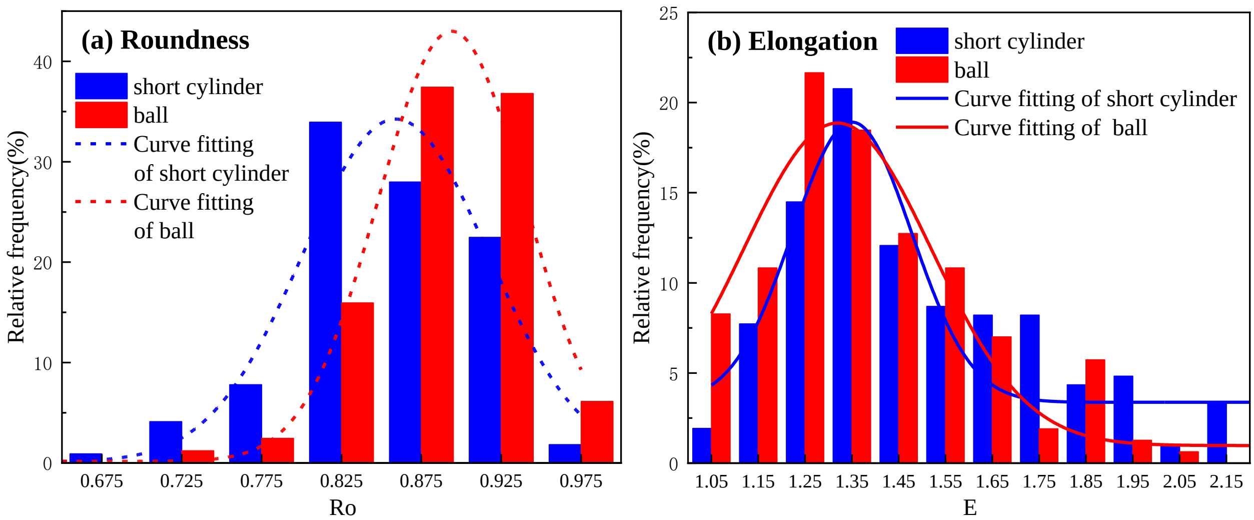

Figure 7. Histogram and fitting curve of the roundness (**a**) and elongation (**b**) for the grinding products.

3.5. DEM Grinding Simulation

The results of particle size distribution in the simulation experiment are shown in Figure 8, which is consistent with the pattern of experimental results. The results show that short cylinder milling produces more intermediate-size particles.

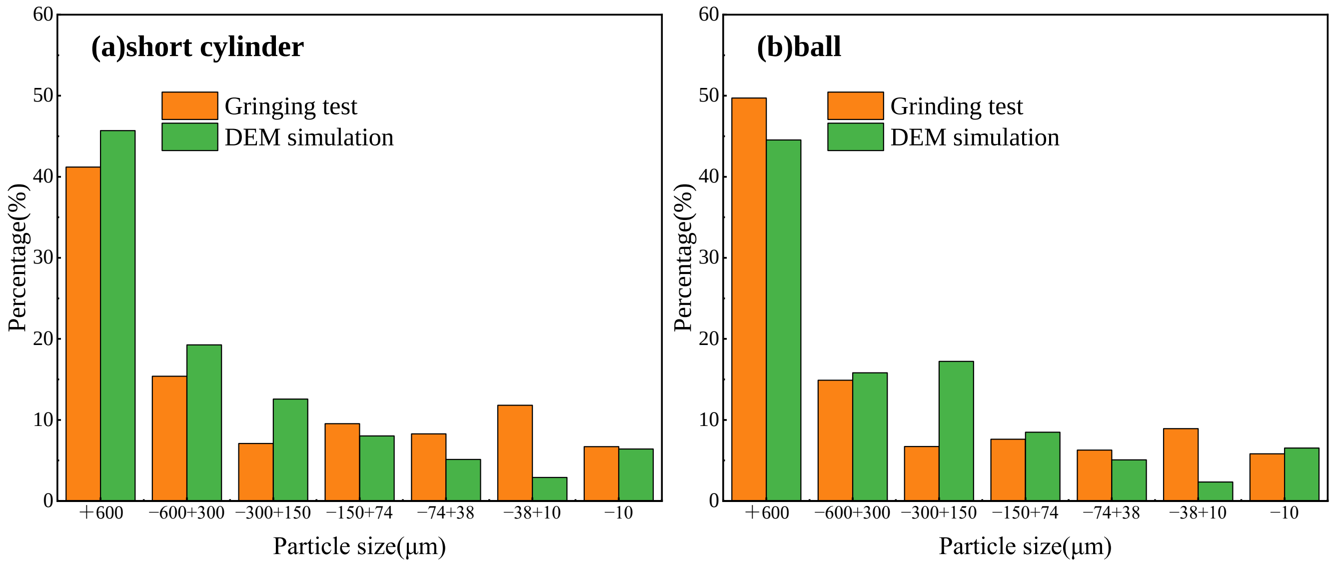

Figure 8. Particle size distribution of test products and simulation products at 5 min using short cylinder (**a**) and ball (**b**) as grinding media.

The simulation results for the sphericity of the ground materials are presented in Figure 9. The simulation results indicate that the sphericity of the short cylinder grinding products is lower compared to the ball grinding products, which is consistent with the experimental observations.

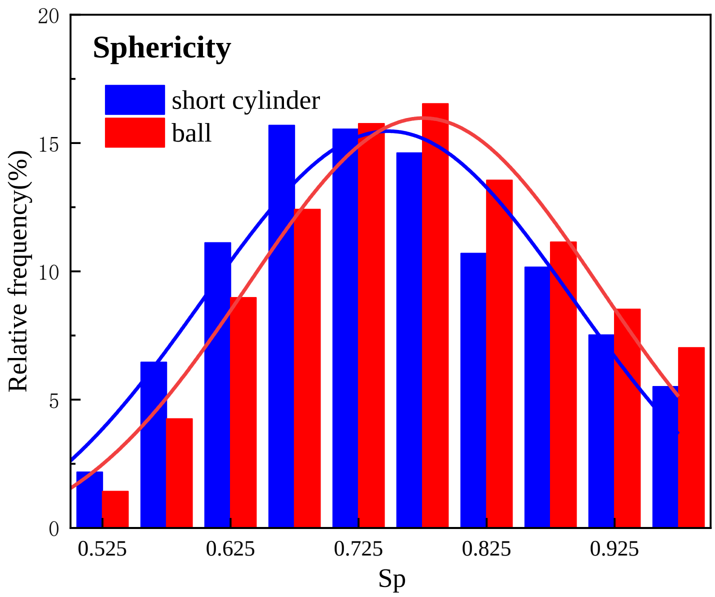

Figure 9. Sphericity of the grinding products of dolomite using short cylinders.

Tables 5 and 6 displayed the distribution of broken fragment sizes observed during the breaking stage in the simulation. It has been observed that the proportion of −74 + 10 μm in the fragmentation distribution of short cylinder grinding products is larger than that of ball milling, and the proportion of −10 μm is smaller than that of ball milling. The simulation results are consistent with the pattern of experimental results.

Table 5. The fragmentation distribution of the dolomite grinding product using short cylinder as grinding media in simulation.

	Product (μm) \ Feed (μm)	−1000 + 600	−600 + 300	−300 + 150	−150 + 74	−74 + 10	−10
Short cylinder	−1000 + 600	0	0	0	0	0	0
	−600 + 300	0.537	0	0	0	0	0
	−300 + 150	0.198	0.444	0	0	0	0
	−150 + 74	0.082	0.266	0.415	0	0	0
	−74 + 10	0.059	0.178	0.419	0.696	0	0
	−10	0.124	0.112	0.166	0.304	1	1

Table 6. The fragmentation distribution of the dolomite grinding product using ball as grinding media in simulation.

	Product (μm) \ Feed (μm)	−1000 + 600	−600 + 300	−300 + 150	−150 + 74	−74 + 10	−10
Ball	−1000 + 600	0	0	0	0	0	0
	−600 + 300	0.597	0	0	0	0	0
	−300 + 150	0.189	0.504	0	0	0	0
	−150 + 74	0.060	0.196	0.413	0	0	0
	−74 + 10	0.038	0.139	0.403	0.595	0	0
	−10	0.117	0.161	0.184	0.405	1	1

3.6. XRD Analysis

Due to the anisotropic nature of the crystal surface, the proportion of the crystal surface exposed may be different for different shapes of particles. This leads to changes in the strength of the interactions between the active sites on the mineral and the reagent. Previous research [34–36] has demonstrated the reliability of X-ray diffraction as a technique for examining crystal surfaces. This method can ascertain the Miller indexes and diffraction peak intensity, which provide insights into the exposed crystal surface [16,19,20,37,38]. Consequently, in this investigation, X-ray diffraction was utilized to assess the exposure proportions of diverse dolomite crystal surfaces in the case of using short cylinders or spherical media. The results are shown in Figure 10, indicating that the {104}, {113} and {018} crystal surfaces are the main exposed surfaces of dolomite, with the {104} crystal surface being particularly prominent.

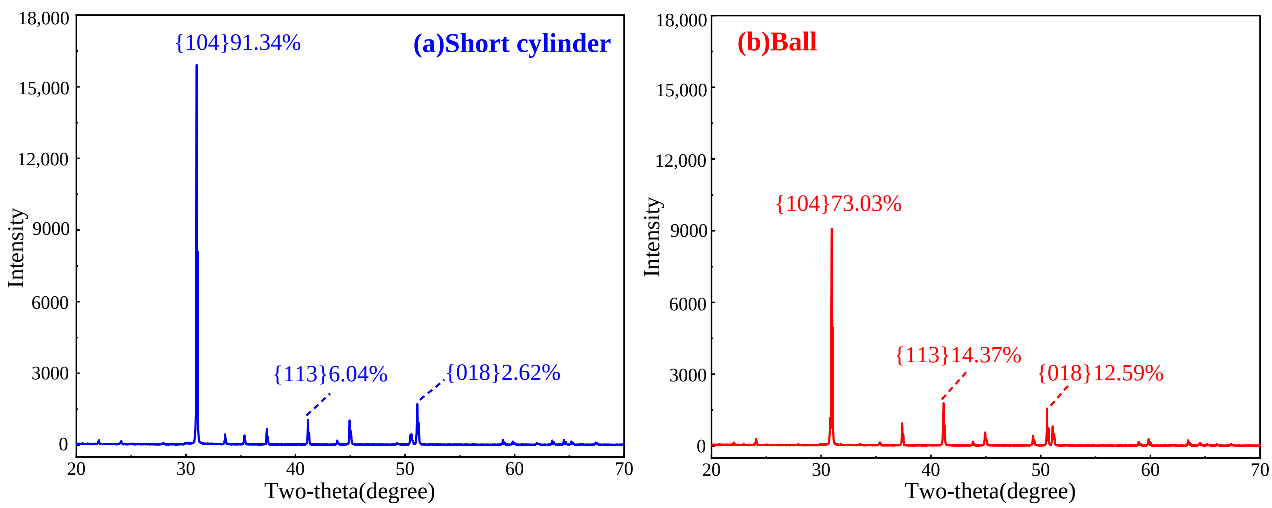

Figure 10. XRD and exposed percentages of dolomite crystal surface of grinding products using short cylinder (**a**) and ball (**b**) media.

To ensure a more precise comparison of the exposure rates of various crystal surfaces, the overall percentage of observed diffraction peaks in the resulting ground products using either short cylinder or spherical media was set as a standard at 100%. The intensities of the four peaks were used to calculate the proportions of the different crystal surfaces that were exposed.

As shown in Figure 10, it was discovered that the proportion of exposed {104} crystal surface of dolomite was greater when employing the short cylindrical media in contrast to the spherical media, while the inverse was observed for the {113} and {018} crystal surface. In Figure 11, the interconnection between the shape of dolomite particles and the proportions of the crystal surface was illustrated. Figure 11 shows that a higher exposure of the {104} surface resulted in a more elongated dolomite particle, denoted as a higher E, which is consistent with the findings of the SEM analysis.

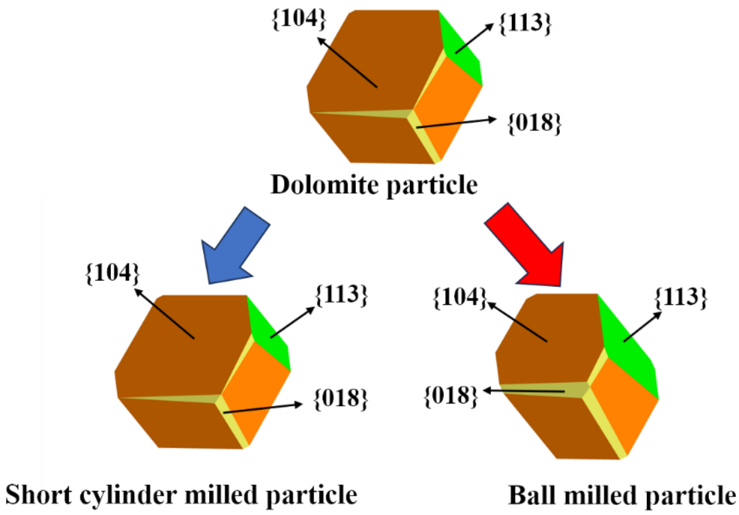

Figure 11. Relationship between the particle morphology and the exposed ratios of crystal surface for grinding products.

3.7. Crystal Chemistry Calculations

XRD analysis showed that the short cylinder mill products exhibited a higher percentage of dolomite {104} surface exposure compared to balls. However, specific changes in the surface chemistry of primary dolomite crystals remain uncertain. Crystal chemistry calculations have been shown in previous studies to be effective for understanding differences in adsorption energy, relaxation degree of crystal surface, dissolution rate, charge on crystal surface, and wettability [39–41].

Table 7 showcases the computed energies and structures observed on different crystal surfaces of dolomite. The data presented in Table 7 unveils the ranking of dolomite's common crystal surface energy, with {018} having the highest energy followed by {113} and {104}. The order aligns with the findings derived from the D_b calculations. The crystal surface with the lowest energy levels was more susceptible to undergoing exposure. This discovery corroborates the XRD findings.

Table 7. The energies of different dolomite crystal surface.

Mineral	Crystal Surface	E_{system} (eV)	$E_{face\ s}$ (J/m^2)
Dolomite (CaMg (CO3)2)	{104}	−19,660.064	0.8931
	{113}	−19,657.926	1.0318
	{018}	−19,652.009	1.6286

The adsorption of reagents onto the exposed metal atoms enables their interaction with the dolomite crystal surface. Crystal structures were utilized to perform calculations for determining the number and density of metal atoms within a given unit cell area. Table 8 exhibits that the {104} crystal surface of dolomite have the highest density of metal atoms (Ca and Mg atoms) in comparison to other crystal surface, suggesting that metal atoms on the {104} crystal surface are more likely to interact with reagents. Thus, to enhance the adsorption of flotation reagents in the grinding and flotation process of dolomite, it could prove advantageous by optimizing the milling process so that a higher percentage of the {104} crystals surface was exposed.

Table 8. The number and density of the exposed metal atoms on different dolomite crystal surface.

Mineral	Crystal Surface	*Az* (nm^2)	Ca and Mg Atoms Number	Ca and Mg Atoms Density (nm^{-2})	D_b (nm^{-2})
Dolomite	{104}	0.3742	4	10.6895	10.6890
	{113}	0.4900	5	10.2041	16.3290
	{018}	0.6014	4	6.6511	16.6277

Dolomite displays a higher percentage of {104} crystal surface exposure during the grinding procedure that utilizes short cylindrical media. Hence, employing short cylinder grinding media proves advantageous in reverse flotation by amplifying the discrepancy in recovery rates between dolomite and fluorapatite, thereby assisting in the efficient separation of these two minerals.

3.8. Flotation Test Results

The results of particle morphology (Figure 7) and crystal chemistry calculations show that dolomite particles produced from short cylindrical media exhibit better floatability than those produced from spherical media. The effects of different shapes of grinding media on the ability of dolomite to float were examined in single-mineral flotation experiments. The single mineral flotation results are illustrated in Figure 12. Based on Figure 12, the flotation recovery of dolomite short cylinder milled products is always higher than that of ball-milled products at pH values ranging from 5.5 to 7. This implies that short cylindrical media is more advantageous for achieving successful flotation of dolomite.

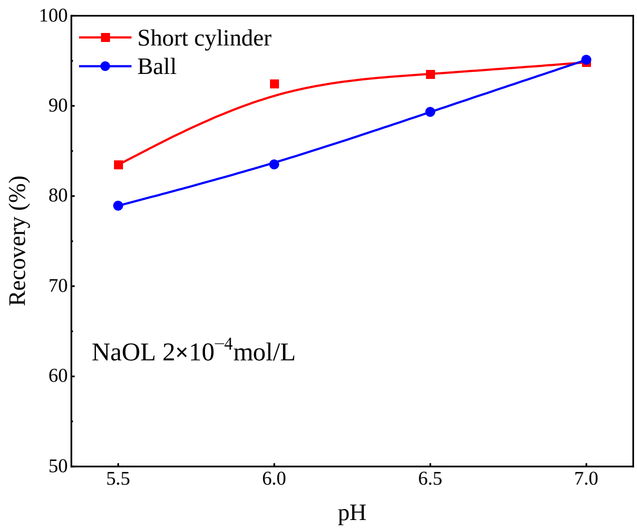

Figure 12. Single mineral flotation results of dolomite ground by short cylinders and balls.

In order to further examine the influence of different shapes of grinding media on dolomite flotation, a comparison was conducted between the flotation outcomes of mixed minerals. The comparison was conducted under the same grinding and flotation conditions, with the sole variation being the shape of the grinding media utilized. In the raw material of the mixed ore flotation in Figure 13, the ratio of fluorapatite and dolomite is 1:1, i.e., P_2O_5

grade is 21.1%. It was prepared by 20 min of short cylinder or ball milling followed by sieving to −74 + 38 μm. As shown in Figure 13, it can be observed that the recovery rates of P_2O_5 in the flotation concentrate differ between the short cylinder-milled products and ball-milled products, with values of 71.6% and 55.7%, respectively. Furthermore, the grade of P_2O_5 in the short cylinder milled product is reported to be 44.5%, which is higher than the grade of P_2O_5 in the ball-milled product. This suggests that leveraging short cylinders as the grinding media is capable of efficiently and selectively grinding fluorapatite while protecting dolomite from overgrinding throughout the grinding procedure. The material that floats during the process of grinding in the short cylinder mill shows a better recovery and higher P_2O_5 grade than that obtained from the ball mill.

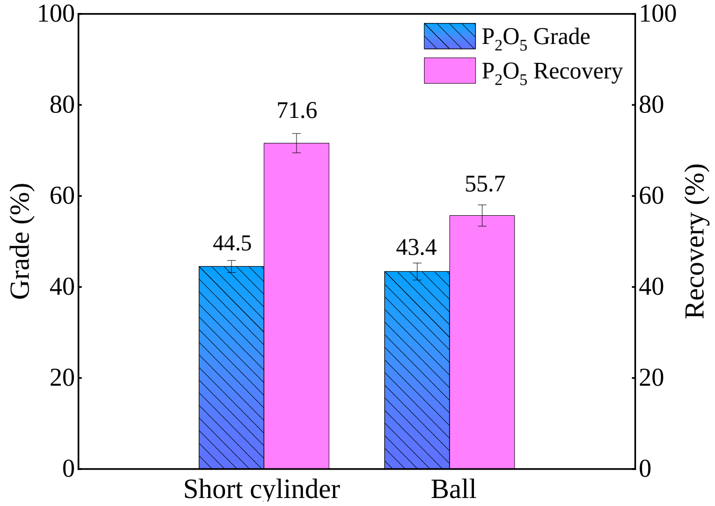

Figure 13. Flotation grade and recovery of P_2O_5 of mixed minerals grinding products.

4. Discussion

The results of the dolomite flotation test (Figures 12 and 13) demonstrated that grinding with short cylinder grinding media had a positive impact on dolomite flotation compared to ball grinding media. This is due to the differences in the physical properties and chemical behavior of dolomite, including particle size distribution, particle shape, and crystal surface reactivity, when it is ground in two different grinding media, short cylinders, and balls.

The modes of contact between the grinding media and the minerals, i.e., point contact and line contact, have been widely observed in various studies [42,43]. When a mineral is in contact with a ball, the contact mode is mainly point contact, resulting in localized pressure on the mineral. This contact often results in mineral particles that are not uniform in size, with some particles being too coarse or too fine. However, when a short cylindrical media is used, the mode of contact with the mineral involves a combination of point and line contact. As a result, the forces applied to the minerals are more evenly distributed, resulting in minerals having uniform sizes and sharper edges (Figures 5–7). These particles exhibit better flotation in the ground product, thereby increasing the ability to adhere to bubbles. In essence, the particle size and shape produced by the short cylindrical media contribute to improved dolomite flotation.

The XRD analysis confirmed that dolomite particles produced with a short cylindrical media showed increased exposure of the {104} crystal surface. Furthermore, dolomite particles ground by short cylindrical media showed the maximum density of metal atoms on the {104} crystal surface, suggesting a greater chance for contact with reagents and subsequent collection. Using DFT (density functional theory) calculations, it was confirmed that the energy on the {104} crystal surface of dolomite was the lowest, thus providing support for this hypothesis. These findings collectively suggest that increasing the exposure of {104} surfaces of dolomite through the use of short cylinder media can effectively enhance dolomite flotation.

5. Conclusions

This comprehensive research investigated the influence of both short cylinder and ball grinding media on the floatability of dolomite, considering various physical and chemical factors such as particle morphology and interface chemistry. Notably, the focus was on how these factors affect the ability of dolomite to be separated through flotation. The findings indicated that dolomite particles ground using short cylindrical media demonstrated a higher recovery of flotation in comparison to those ground using spherical media. The enhanced flotation efficiency is due to the short cylinders' capability to produce more elongated particles with intermediate sizes and sharp edges. Furthermore, the use of short cylindrical media in grinding dolomite particles increased the exposure of {104} crystal surface, which enhances their ability to interact with collectors, resulting in effective flotation. The experimental results are consistent with the Population Balance Model and computer-based simulation results of the DEM grinding.

The discrepancies in how short cylinders and balls interact with dolomite during grinding can be ascribed to the contrasting contact modes displayed by the grinding media. Short cylindrical media come into contact with dolomite in a manner that involves both points and lines. This interaction brings about numerous benefits including the reduction in coarse particles, avoidance of excessive grinding, and exposure of higher active crystal surface. As a result, employing short cylindrical media allows for a targeted grinding process for dolomite, leading to enhanced floatability. The use of short cylinders shows promise in enhancing the efficiency of dolomite grinding and flotation procedures.

Author Contributions: S.R.: Methodology, Validation, Formal analysis, Investigation, Data curation, Writing—original draft, Visualization. C.W.: Methodology, Formal analysis, Data curation, Visualization. Z.G.: Methodology, Validation, Writing—review & editing, Visualization. S.X.: Conceptualization, Methodology, Validation, Visualization, Resources, Supervision, Project administration, Funding acquisition. All authors have read and agreed to the published version of the manuscript.

Funding: This research was funded by the National Key R&D program of China (2022YFC2904702), the Key Program for International S&T Cooperation Projects of China (2021YFE0106800), the Leading Talents of S&T Innovation of Hunan Province, China (2021RC4002), the Science Fund for Distinguished Young Scholars of Hunan Province, China (2020JJ2044), the Key Research and Development Program of Hunan Province, China (2021SK2043), the National 111 Project, China (B14034).

Data Availability Statement: Data will be made available on request.

Conflicts of Interest: The authors declare that they have no known competing financial interests or personal relationships that could have appeared to influence the work reported in this paper.

References

1. Koppelaar, R.H.E.M.; Weikard, H.P. Assessing phosphate rock depletion and phosphorus recycling options. *Glob. Environ. Chang.* **2013**, *23*, 1454–1466. [CrossRef]
2. Rubel Biswas, C.; Graham, A.M.; Anthony, J.W.; Arora, M. A review of recent substance flow analyses of phosphorus to identify priority management areas at different geographical scales. *Resour. Conserv. Recycl.* **2014**, *83*, 213–228.
3. Amirech, A.; Mustapha, B.; Kouachi, S. Two-stage reverse flotation process for removal of carbonates and silicates from phosphate ore using anionic and cationic collectors. *Arab. J. Geosci.* **2018**, *11*, 593. [CrossRef]
4. Huang, W.; Liu, W.; Zhong, W.; Chi, X.; Rao, F. Effects of common ions on the flotation of fluorapatite and dolomite with oleate collector. *Miner. Eng.* **2021**, *174*, 107213. [CrossRef]
5. Zhang, J.; Li, H.; Chai, Y.; Zhang, Q. Crystal properties and interaction with flotation reagent of fluorapatite and dolomite. *Miner. Eng.* **2023**, *201*, 108204. [CrossRef]
6. Yu, H.; Zhu, Y.; Lu, L.; Hu, X.; Li, S. Removal of dolomite and potassium feldspar from apatite using simultaneous flotation with a mixed cationic-anionic collector. *Int. J. Min. Sci. Technol.* **2023**, *33*, 783–791. [CrossRef]
7. Wei, Z.; Zhang, Q.; Wang, X. New insights on depressive mechanism of citric acid in the selective flotation of dolomite from apatite. *Colloids Cryst. Surf. A Physicochem. Eng. Asp.* **2022**, *653*, 130075. [CrossRef]
8. Liu, X.; Ruan, Y.; Li, C.; Cheng, R. Effect and mechanism of phosphoric acid in the apatite/dolomite flotation system. *Int. J. Miner. Process.* **2017**, *167*, 95–102. [CrossRef]
9. Kaba, O.B.; Filippov, L.O.; Filippova, I.V.; Badawi, M. Interaction between fine particles of fluorapatite and phosphoric acid unraveled by crystal surface spectroscopies. *Powder Technol.* **2021**, *382*, 368–377. [CrossRef]

10. Mohammadkhani, M.; Noaparast, M.; Shafaei, S.Z.; Amini, A.; Amini, E.; Abdollahi, H. Double reverse flotation of a very low grade sedimentary phosphate rock, rich in carbonate and silicate. *Int. J. Miner. Process.* **2011**, *100*, 157–165. [CrossRef]
11. Bulatovic, S.M. Chapter 26—Flotation of Phosphate Ore. In *Handbook of Flotation Reagents: Chemistry, Theory and Practice*; Bulatovic, S.M., Ed.; Elsevier: Amsterdam, The Netherlands, 2015; pp. 1–19.
12. Qian, H.Y.; Kong, Q.G.; Zhang, B.L. The effects of grinding media shapes on the grinding kinetics of cement clinker in ball mill. *Powder Technol.* **2013**, *235*, 422–425. [CrossRef]
13. Shi, F. Comparison of grinding media—Cylpebs versus balls. *Miner. Eng.* **2004**, *17*, 1259–1268. [CrossRef]
14. Qingfei, X.; Bo, L.; Huaibin, K. The Effect of Fine Grinding Media Feature on Grinding Results. *AASRI Procedia* **2014**, *7*, 120–125.
15. Yekeler, M.; Ulusoy, U.; Hiçyilmaz, C. Effect of particle shape and roughness of talc mineral ground by different mills on the wettability and floatability. *Powder Technol.* **2004**, *140*, 68–78. [CrossRef]
16. Chengwei, L.; Zhiyong, G. Tune crystal surface physicochemical property of fluorite particles by regulating the exposure degree of crystal surface. *Miner. Eng.* **2018**, *128*, 123–132.
17. Wotruba, H.; Hoberg, H.; Schneider, F.U. Investigations on the Separation of Microlithe and Zircon—The Influence of Particle Shape on Floatability. In Proceedings of the XVII International Mineral Processing Congress, Dresden, Germany, 83–95 January 1991.
18. Huh, C.; Mason, S.G. The flotation of axisymmetric particles at horizontal liquid interfaces. *J. Colloid Interface Sci.* **1974**, *47*, 271–289. [CrossRef]
19. Chengwei, L.; Zhiyong, G. Effect of grinding media on the crystal surface property and flotation behavior of scheelite particles. *Powder Technol.* **2017**, *322*, 386–392.
20. Wang, C.; Deng, J.; Tao, L.; Sun, W.; Xiao, Q.; Gao, Z. Enhanced flotation of chalcopyrite particles by grinding with short cylindrical media. *Miner. Eng.* **2022**, *188*, 107827. [CrossRef]
21. Meng, J.; Xu, L.; Luo, L.; Shu, K. Effects of grinding media on the flotation behavior of spodumene in mixed anionic/cationic collectors system. *Colloids Cryst. Surf. A Physicochem. Eng. Asp.* **2021**, *627*, 127213. [CrossRef]
22. Henri, B.; John, D. A new estimation technique for the determination of breakage and selection parameters in batch grinding. *Powder Technol.* **1997**, *94*, 173–179.
23. Cundall, P.A.; Strack, O.D.L. A discrete numerical model for granular assemblies. *Geotechnique* **1979**, *29*, 47–65. [CrossRef]
24. Walton, O.R.; Braun, R.L. Stress calculations for assemblies of inelastic speres in uniform shear. *Acta Mech.* **1986**, *63*, 73–86. [CrossRef]
25. Weerasekara, N.S.; Powell, M.S.; Cleary, P.W.; Tavares, L.M.; Evertsson, M.; Morrison, R.D.; Quist, J.; Carvalho, R.M. The contribution of DEM to the science of comminution. *Powder Technol.* **2013**, *248*, 3–24. [CrossRef]
26. Gao, Z.; Fan, R.; Ralston, J.; Sun, W.; Hu, Y. Crystal surface broken bonds: An efficient way to assess the crystal surface behaviour of fluorite. *Miner. Eng.* **2019**, *130*, 15–23. [CrossRef]
27. Weifan, D.; Xianbo, L. Insight into the inhibition mechanism of carboxymethyl cellulose for flotation of dolomite and fluorapatite: Experimental and DFT studies. *Colloids Cryst. Surf. A Physicochem. Eng. Asp.* **2023**, *674*, 131957.
28. Gontijo, C.; Fornasiero, D.; Ralston, J. The Limits of Fine and Coarse Particle Flotation. *Can. J. Chem. Eng.* **2008**, *85*, 739–747. [CrossRef]
29. Jameson, G.J. Advances in Fine and Coarse Particle Flotation. *Can. Metall. Q.* **2010**, *49*, 325–330. [CrossRef]
30. Ahn, J.H.; Gebhardt, J.E. Effect of grinding media-chalcopyrite interaction on the self-induced flotation of chalcopyrite. *Int. J. Miner. Process.* **1991**, *33*, 243–262. [CrossRef]
31. Crawford, R.; Ralston, J. The influence of particle size and contact angle in mineral flotation. *Int. J. Miner. Process.* **1988**, *23*, 1–24. [CrossRef]
32. Multani, R.S.; Waters, K.E. Flotation recovery–by–size comparison of pyrrhotite superstructures with and without depressants. *Miner. Eng.* **2019**, *130*, 92–100. [CrossRef]
33. Kursun, H.; Ulusoy, U. Influence of shape characteristics of talc mineral on the column flotation behavior. *Int. J. Miner. Process.* **2006**, *78*, 262–268. [CrossRef]
34. Davey, R.J.; Mullin, J.W.; Whiting, M.J.L. Habit modification of succinic acid crystals grown from different solvents. *J. Cryst. Growth* **1982**, *58*, 304–312. [CrossRef]
35. Gao, Z.; Xie, L.; Cui, X.; Hu, Y.; Sun, W.; Zeng, H. Probing Anisotropic Crystal surface Properties and Crystal surface Forces of Fluorite Crystals. *Langmuir* **2018**, *34*, 2511–2521. [CrossRef] [PubMed]
36. Lovette, M.A.; Browning, A.R.; Griffin, D.W.; Sizemore, J.P.; Snyder, R.C.; Doherty, M.F. Crystal Shape Engineering. *Ind. Eng. Chem. Res.* **2008**, *47*, 9812–9833. [CrossRef]
37. Cao, A.; Xu, C.; Liang, J.; Wu, D.; Wei, B. X-ray diffraction characterization on the alignment degree of carbon nanotubes. *Chem. Phys. Lett.* **2001**, *344*, 13–17. [CrossRef]
38. Mclaren, A.; Valdes-Solis, T.; Li, G.; Tsang, S.C. Shape and size effects of ZnO nanocrystals on photocatalytic activity. *J. Am. Chem. Soc.* **2009**, *131*, 12540–12541. [CrossRef]
39. Gao, Z.-Y.; Sun, W.; Hu, Y.-H.; Liu, X.W. Anisotropic crystal surface broken bond properties and wettability of calcite and fluorite crystals. *Trans. Nonferrous Met. Soc. China* **2012**, *22*, 1203–1208. [CrossRef]
40. Kupka, N.; Rudolph, M. Froth flotation of scheelite—A review. *Int. J. Min. Sci. Technol.* **2018**, *28*, 373–384. [CrossRef]

41. Ribeiro, R.A.P.; Andrés, J.; Longo, E.; Lazaro, S.R. Magnetism and multiferroic properties at MnTiO3 crystal surface: A DFT study. *Appl. Cryst. Surf. Sci.* **2018**, *452*, 463–472. [CrossRef]
42. Ulusoy, U.; Yekeler, M. Correlation of the surface roughness of some industrial minerals with their wettability parameters. *Chem. Eng. Process.* **2005**, *44*, 555–563. [CrossRef]
43. Ulusoy, U.; Kursun, I. Comparison of different 2D image analysis measurement techniques for the shape of talc particles produced by different media milling. *Miner. Eng.* **2011**, *24*, 91–97. [CrossRef]